Published in final edited form as:
Nat Cell Biol. 2019 October ; 21(10): 1286–1299. doi:10.1038/s41556-019-0392-4.

Functional transcription promoters at DNA double-strand breaks mediate RNA-driven phase separation of damage response factors

Fabio Pessina[1], **Fabio Giavazzi**[2], **Yandong Yin**[3], **Ubaldo Gioia**[1], **Valerio Vitelli**[1], **Alessandro Galbiati**[1], **Sara Barozzi**[1], **Massimiliano Garre**[1], **Amanda Oldani**[1], **Andrew Flaus**[4], **Roberto Cerbino**[2], **Dario Parazzoli**[1], **Eli Rothenberg**[3], **Fabrizio d'Adda di Fagagna**[1,5,*]

[1]IFOM-The FIRC Institute of Molecular Oncology, Milan 20139, Italy [2]Università degli Studi di Milano, Dipartimento di Biotecnologie Mediche e Medicina Traslazionale, 20090 Segrate, Italy [3]Department of Biochemistry and Molecular Pharmacology, New York University School of Medicine, New York, NY, USA [4]Centre for Chromosome Biology, Biochemistry, School of Natural Sciences, National University of Ireland Galway, Ireland [5]Istituto di Genetica Molecolare, CNR - Consiglio Nazionale delle Ricerche, Pavia 27100, Italy

Abstract

Damage-induced long non-coding RNAs (dilncRNA) synthesized at DNA double-strand breaks (DSBs) by RNA polymerase II (RNAPII) are necessary for DNA damage response (DDR) foci formation. We demonstrate that induction of DSBs results in the assembly of functional promoters that include a complete RNAPII pre-initiation complex (PIC), MED1 and CDK9. Absence or inactivation of these factors causes DDR foci reduction both *in vivo* and in an *in vitro* system that reconstitutes DDR events on nucleosomes. We also show that dilncRNAs drive molecular crowding of DDR proteins such as 53BP1 into foci that exhibit liquid-liquid phase separation (LLPS) condensate properties. We propose that the assembly of DSB-induced transcriptional promoters drives RNA synthesis which stimulates phase separation of DDR factors in the shape of foci.

*Corresponding author: fabrizio.dadda@ifom.eu.

Author Contribution

F.G. conceived and performed all LLPS analysis of 53BP1 foci. Y.Y. performed all STORM experiments. U.G. performed, together with M.G., timelaps experiments of 53BP1 foci treated with NH_4OAc and 1,6-hexanediol, performed comet assays and the EJ5 repair assays. V.V. conceived and performed strand-specific RT-qPCR and qPCR analysis of ChIP experiments and dilncRNA detection both in cells and *in vitro*. A.G. conceived and performed DIPLA analysis. S.B. performed all microinjections in cells and all 53BP1 droplets detection experiments *in vitro*. M.G. performed all timelaps experiments assisted by U.G. F.P., performed all FRAP experiments and confocal analysis of 53BP1 foci formation. A.O. performed all quantifications of confocal images. A.F. supervised F.P. for the *in vitro* system and nucleosome preparation and edited the manuscript. R.C. advised F.G. and edited the manuscript. D. P. supervised S.B. M.G. A.O. and advised them on all imaging experiments. E.R. supervised Y.Y. and edited the manuscript. F.P. designed and performed all remaining experiments and wrote the manuscript. F.d'A.d.F conceived the study and, together with F.P., assembled and revised the manuscript. All authors commented on the manuscript.

Competing Financial Interests

The Authors have no financial or non-financial competing interests. F.d'A.d.F. is inventor of the patent application: PCT/EP2013/059753

Europe PMC Funders Author Manuscripts

DNA lesions occur constantly and failure to properly recognize and repair this damage can result in genome instability, cellular senescence or cell death [1, 2]. Evolutionarily-conserved mechanisms collectively known as the DNA damage response (DDR) detect DNA damage, signal its presence, and facilitate repair. DNA double-strand breaks (DSBs) are a particularly dangerous class of lesions in which both DNA strands are cleaved [3]. The DDR at DSBs is triggered by recognition of exposed DNA ends by the sensor complex MRE11-RAD50-NBS1 (MRN) which recruits the apical protein kinase ATM to phosphorylate the histone variant H2AX at serine 139, forming γH2AX. This favours the accumulation of several proteins such as MDC1 and 53BP1 at sites of DNA damage in globular, cytologically-detectable structures known as DDR foci where signalling and repair reactions occur. Recently, we reported that DSBs recruit RNA polymerase II (RNAPII) in a MRN-dependent manner to synthesize damage-induced long non-coding RNA (dilncRNA), that can be processed into shorter DDR RNA (DDRNA), which interact with DDR factors such as 53BP1 to accumulate them at DSBs as DDR foci [4–6]. dilncRNA and DDRNA contribute to DNA repair [5, 7], and at resected DNA ends dilncRNA can form DNA:RNA hybrids favouring DNA repair by homologous recombination [8, 9]. We and others have shown that DDR foci disassemble upon RNase A treatment [4, 10, 11], that RNAPII inhibitors prevent focus formation and DNA repair [5], and that antisense oligonucleotides against dilncRNA and DDRNA generated at individual DSBs can inhibit focus formation and DSB repair in a sequence-specific manner [5]. Despite this evidence, it is unknown whether DSBs recruit factors commonly engaged at canonical promoters and whether they are necessary for dilncRNA synthesis and DDR focus formation. Promoters typically recruit a machinery comprising of RNAPII and six general transcription factor complexes (TFIIA, TFIIB, TFIID, TFIIE, TFIIF and TFIIH) known collectively as the Pre-Initiation Complex (PIC), although transcription initiation can also occur without canonical promoter sequences [12]. In addition, studies of the Mediator complex, a transcription co-activator factor that participates in almost all PIC activities, blurred the difference between promoters and enhancers [13–15]. Recently, it has been reported that the activity of super-enhancers and DNA binding transcription factors is dependent on liquid-liquid phase separation (LLPS) events [16–20], a process involving the spontaneous organization of a solution into two phases with different densities[21–24]. RNA is a common agent recognised to drive the formation of such biomolecular condensates providing means to compartmentalize and concentrate biochemical reactions [22–28] and multivalent interactions, a feature of RNA, and intrinsically disordered regions of proteins have been proposed to promote liquid-liquid phase-separation [23, 26, 29, 30]. In addition, at sites of DNA damage some RNA binding proteins have been reported to be rapidly but transiently recruited and to undergo liquid demixing promoted by poly(ADP-ribose) (PAR)[31, 32]. We thus tested whether non-coding RNA (ncRNA) generated at DSBs had a role in LLPS leading to DDR foci formation and maturation.

Here we show, both *in vivo* and *in vitro*, that general transcription factors, normally involved at gene promoters in RNAPII regulation, are necessary for dilncRNA synthesis at sites of break and that dilncRNAs, together with γH2AX, drive LLPS of DDR factors in the form of DDR foci.

Results

DSB generation leads to recruitment of the PIC, MED1 and CDK9 together with RNAPII

We previously reported that POLR2A, the catalytic component of RNAPII, is recruited to DNA ends both *in vitro* in cell extracts and *in vivo* in cultured cells [5]. To test whether the PIC and associated components MED1 and CDK9 (collectively here referred to as PMC) are recruited to DSBs *in vivo,* we performed chromatin immunoprecipitations (ChIP) at an endogenous locus in HeLa cells that can be cleaved by the sequence-specific I-PpoI endonuclease [5], or within a chromosomally-integrated artificial construct that can be targeted by I-SceI meganuclease [5]. As a positive control, we used the actin gene promoter (Fig. S1a). We mapped the association of the main subunits of PMC and RNAPII by ChIP at 100 bp, 2000 bp, 3000 bp from the break before or after DSB induction. γH2AX was detected at all sites upon DSB. Interestingly, in both systems, all tested PMC components and RNAPII were robustly associated at 100 bp from the DSB upon its generation. Differently, at 2000 bp only RNAPII was detected, while at 3000 bp neither PMC nor RNAPII were detectable (Fig. 1a, b, Fig. S1b). In a different *in vitro* system, in which DNA oligonucleotides were immobilized on streptavidin beads and incubated with HeLa nuclear extract (Fig. S1c) RNAPII (POLR2A) and all PMC components tested were found associated to DNA ends, regardless of their structure (3’ or 5’ 10 nt overhangs or blunt; Fig. S1c, d, e).

To test genome-wide the recruitment of PIC and RNAPII, we used super-resolution imaging in cells treated with the DSB-inducing agent neocarzinostatin (NCS). We therefore determined the degree of co-localization between TBP (a TFIID component) or CDK7 (a TFIIH component), the first and the last PIC components recruited to transcriptional promoters, respectively [33], with γH2AX by STochastic Optical Reconstruction Microscopy (STORM) [34, 35] (Fig. 2a-d). As negative controls we used both the correlation of signals from two uncorrelated, randomly picked, nuclei (Fig. 2e), and the correlation between γH2AX and MCM6, an abundant DNA replication factor (Fig. 2d and f). As shown in Figure 2e and f, γH2AX signals colocalized with POLR2A active form POLR2A-pS5. In addition, we observed a significant co-localization of TBP and CDK7 with γH2AX in damaged cells (Fig. 2b and c) and in untreated cells experiencing endogenous low DNA damage levels (Fig. S2a-c, g and h). We also pulsed cells with ethynyl uridine (EU) to detect nascent transcripts following DSB generation. By calculating the correlation in treated versus untreated cells, we confirmed that EU-γH2AX co-localization levels increased in NCS-treated cells proportionally with increased γH2AX signal (Pearson coefficient 0.31, Fig. S2l) and that ~50% of γH2AX signals colocalized with EU (Fig. 2g, Fig S6) – likely an underestimation given a 3% substitution rate of uridine with EU[36].

To independently validate the proximity of PIC components to DSB DNA ends, we exploited DNA damage *In situ* ligation followed by Proximity Ligation Assay (DI-PLA) [37, 38]. DI-PLA confirmed that TBP, TFIIB, CDK7 and γH2AX are all in close proximity to DNA ends in cells exposed to ionizing radiation, while the abundant Cyclin A is not (Fig. 2h, Fig. S2m).

Altogether, these independent approaches consistently indicate that PMC components and RNAPII assemble at DSBs and coexist with local RNA synthesis.

RNAPII localization to DSBs is dependent on PIC and MRN

To test the role of PIC on recruitment or stabilization of RNAPII at DSBs, we knocked down TBP, or MRN as control (Fig. S3a), and monitored RNAPII association to a genomic DSB by ChIP as in Fig. 1a. We observed that accumulation of total and active RNAPII at DSB was strongly inhibited upon TBP knockdown, comparable to MRN loss (Fig. 3a). Similar to their assembly at promoters [33] CDK7 recruitment depends on TBP. In addition, TBP and CDK7 depend on MRN but not vice versa (Fig. 3a). TBP knockdown strongly inhibited dilncRNA synthesis, similarly to MRN inactivation, indicating a crucial role of PIC components in dilncRNA synthesis (Fig. 3b).

Since PIC recruitment and function is impaired upon MRN knockdown, we next tested whether this effect could be mediated by their biochemical interaction. We observed that MRN complex immunoprecipitation with antibodies against RAD50 pulled down PIC components tested together with RNAPII. Conversely, TBP immunoprecipitated MRN as well as POLR2A. Some interactions were stronger when performed in extracts from irradiated cells (Fig. 3c).

These results are consistent with a model in which MRN acts as a tethering factor at DSB for PIC with which it forms a complex. Lack of PIC prevents POLR2A accumulation or retention at DSB and, consequently, dilncRNA synthesis.

PIC inactivation by RNA interference, pharmacological inhibition or inhibitory antibodies reduces DDR signalling in cells

To determine the functional contribution of PIC to DDR activation at DSBs, we individually knocked down TBP and TFIIB, in order to prevent PIC assembly and monitored DDR foci formation. We observed that cells with reduced levels of TBP or TFIIB showed reduced 53BP1, phosphorylated ATM (pATM) and MDC1 foci formation upon ionizing radiation (Fig. 4a, Fig. S4a, b) despite unaltered DDR proteins levels (Fig. S3b). Expression of knockdown-resistant alleles of TBP and TFIIB restored foci formation (Fig. S4c). γH2AX foci formation was unaffected in number, with a small reduction in intensity. Consistent with these results, TBP or TFIIB knockdown reduced RNA synthesis at DSB (Fig. S4d, S3b) and of canonical transcription (Fig. S4e). Since prolonged knockdown of PIC components could alter the expression of cellular genes and indirectly impact on DDR, we acutely inhibited PIC functions by treating cells with THZ1, a small-molecule CDK7-inhibitor [39] for 30 minutes, irradiated them and fixed them for immunofluorescence 15 minutes later. Pharmacological inhibition of CDK7 resulted in a reduction of pATM and 53BP1 foci number comparable to that observed with an ATM inhibitor and to 5,6-dichloro-1-β-D-ribofuranosylbenzimidazole (DRB), a CDK7/9 inhibitor (Fig. 4b, Fig. S4f). To independently strengthen our conclusions and further reduce the time between PIC inactivation and the study of its impact on DDR, we inactivated PIC components by nuclear microinjection of antibodies against regulatory domains of TBP or TFIIB, a validated approach [40, 41], or against the FLAG epitope as negative control. Cells were microinjected,

irradiated 20 minutes afterwards, and fixed and stained for DDR markers after 15 additional minutes. We observed that irradiated cells microinjected with TBP or TFIIB antibodies showed impaired 53BP1 and pATM focus formation, whereas FLAG antibody-injected cells remained unaffected (Fig. 4c).

Together, these observations generated using three independent strategies demonstrate that inactivation of PMC consistently results in diminished DDR activation in the form of DDR foci.

Accumulation of DDR factors at chromatinised DNA ends *in vitro* is boosted by PIC-dependent local RNA synthesis

To study the role of PIC and transcription on DDR factors recruitment and activation at DNA ends in the absence of potential indirect gene expression alterations, we developed an *in vitro* system to recapitulate the recruitment of DDR factors at DSB as observed in living cells. We assembled a DNA fragment with biotin at both ends into nucleosomes using recombinant core histone octamers containing either histone H2A or H2AX. These chromatinized arrays were immobilized on streptavidin-coated beads and cleaved, or mock treated, by I-SceI generating DNA fragments with free DNA ends (Fig. 5a). The intact or cleaved beads-bound nucleosomes were incubated with HeLa nuclear extract that had been precleared of chromatin and free of rNTPs, thus making transcription dependent on exogenously-added rNTPs. We incubated uncut or cut nucleosome arrays with nuclear extract and rATP and rGTP to provide energy to the system without allowing transcription (Fig. 5b, e). Under these conditions, we observed MRN, ATM and POLR2A binding as well as PMC accumulation only on chromatin bearing DNA ends. Despite γH2AX generation, MDC1, 53BP1 or pATM could not be robustly detected in association with cut chromatin. When the entire rNTP pool was supplied and RNA synthesis was allowed (Fig. 5b, e), a strong H2AX-dependent accumulation of MDC1, 53BP1 and pATM was observed on cut nucleosome arrays. The observed accumulation of DDR factors (secondary recruitment) that is not only γH2AX-dependent but also transcription-dependent is consistent with our observations in cells. In addition, since PIC and RNAPII recruitment to cut nucleosomes was independent of RNA synthesis, while rNTP were necessary for secondary DDR factors recruitment, the contribution of PMC and RNAPII to DDR likely depends on their ability to support RNA synthesis (Fig. 5b, e). To further probe the requirement for RNA synthesis, we treated our reactions with RNaseA to degrade RNA, or DRB or α-amanitin to prevent RNA synthesis (Fig 5c, e). All three treatments prevented DDR factors secondary recruitment despite no impact on γH2AX (Fig. 5c), consistent with results above.

Having validated this system, we used it to test the role of PIC. We thus included, in our reactions, inhibitory antibodies raised against regulatory domains of TBP or TFIIB, or FLAG as negative control, as previously used in cells (Fig. 4c). We observed that antibodies against TBP or TFIIB prevented recruitment of downstream PMC components, such as CDK7, MED1 and CDK9 to DSBs, and this in turn reduced pATM, 53BP1 and MDC1 recruitment despite unchanged γH2AX levels (Fig. 5d). Furthermore, PIC inhibition reduced dilncRNA levels (Fig. 5e).

In summary, we established and validated an *in vitro* nucleosome array system that recapitulates tested DDR activation and transcriptional events occurring at DSBs in cells. By exploiting this system, we demonstrated that RNA synthesis, supported by PIC components, is essential for H2AX-dependent recruitment of DDR factors.

53BP1 foci at DSB exhibit liquid-like phase separation characteristics

DDR foci are membraneless globular nuclear bodies. The results shown here and those previously published [4, 5, 11] indicate that their formation depends on RNA molecules generated at DSB. Recently, a number of intracellular structures have been shown to be generated by protein LLPS promoted by RNA [22–28]. Hence, we hypothesised that PMC-supported RNA synthesis by RNAPII at DSB could facilitate LLPS of DDR factors in the form of DDR foci. 53BP1 is a major component of DDR foci whose accumulation at DSB has been shown to be dynamic [42] and RNA-dependent [4–6, 10]. 53BP1 protein contains both short low complexity regions and long intrinsically disordered regions (Fig. S5a, b), as well as high content of serines and charged regions known to facilitate condensates formation [23, 24]. A hallmark of liquid-like condensates is a fast and homogeneous internal dynamic reorganization and rapid exchange between phases which can be observed by fluorescence recovery after photobleaching (FRAP) [23–25]. We therefore used U2OS cells stably expressing near-endogenous levels of 53BP1 fused to GFP [42] and photobleached individual 53BP1-GFP foci at different time points post-irradiation to test whether they showed liquid-like behaviours. We observed a fast and homogeneous recovery within 7-20 seconds comparable to previously-reported liquid compartments [17, 18, 23, 43] (Fig. 6a). This behaviour seemed to evolve with time and this was not due to progressive foci size increase since by bleaching only a small area of fixed size at the centre of foci at different time point an increase in FRAP recovery time was observed (Fig. 6b *i* and *ii*) confirming a progressive increase in internal viscosity, as previously reported for other bodies [23–25, 31].

From the diffusion coefficient of 53BP1 molecules within foci we estimated an average viscosity of 2.5 Pa·s (see Methods for further details): this value, similar to glycerol[44], is 500 times larger than that of the nucleoplasm. Recent reports showed that RNA is able to modulate in a sequence-dependent manner viscoelastic properties of condensates and in particular to promote faster exchange rate and prevent fast maturation [45, 46]. We therefore tested whether de novo transcription could be functional in regulating liquid properties of 53BP1 foci too. Upon treatment with THZ1, 53BP1 foci showed markedly slower recovery times in FRAP experiments, suggesting that RNA favours 53BP1 internal mobility and thus liquid-like behavior (Fig. 6b *iii* and *iv*). Ammonium acetate (NH_4OAc) has been used to target RNA foci [43], and 1,6-hexanediol [47] to perturb liquid-like droplets [48]. Upon NH_4OAc treatment, 53BP1 foci completely dissolved within seconds and promptly reformed upon wash out (Movie 1, Fig. 6c and d); similarly, 1,6-hexanediol severely reduced 53BP1 foci intensity (Fig. 6c).

Next, to determine the biophysical properties of 53BP1 foci, we performed live cell analysis of the dynamics and morphology of individual foci after IR. During the first 100 minutes, the number and average focal radius of detected foci per nucleus increased over time (Fig. 7a *i-ii*). Subsequently, a decrease in the total number of foci N_{foci} but an increase in average

focal radius $\langle R \rangle$ were observed due to progressive coalescence or ripening of smaller foci (Movie 2 and 3, Fig. 7a, a *iii-iv*, b) while the total volume of mature 53BP1 foci per nucleus remained constant (Fig. 7a *v*). Such a progression of nucleation, growth and coarsening is a characteristic of binary fluid phase separation with a low volume fraction in the transformed phase [25, 49–51]. The asymptotic behaviours of N_{foci} and $\langle R \rangle$ as a function of time can inform on the processes driving coarsening [21, 50, 52]. The observed combination of $N_{foci} \sim t^{-0.8\pm0.2}$ and $\langle R \rangle \sim t^{0.29\pm0.05}$ is compatible with both Diffusion Limited Coarsening (DLC) and Brownian Motion Coalescence (BMC) [21, 50, 52]. However, the majority of droplets disappear without physical contact, suggesting that DLC could be the dominant process (Fig. 7a *vi*). An additional characteristic of liquid-liquid interfaces is surface-tension driven fluctuations (capillary waves [53]). Measurements of spontaneous shape fluctuations of 53BP1 foci (Fig. S5c *i-iii*) were consistent with capillary waves in an overdamped regime [54] (Fig. 7d *i*). The characteristic lifetime τ of the shape fluctuations scales linearly with the size R of 53BP1 foci: $\tau \cong cR$ (Fig. 7d *ii*), strongly supporting a model of shape fluctuations due to capillary waves on the surface of a viscous droplet, with $c \cong \eta/\gamma$ [55]. Combining our estimates of internal viscosity and fluctuation lifetime, we calculated that the effective surface tension of 53BP1 foci is very low: $\gamma \cong 0.5\ \mu N/m$, similar to P granules [56].

We next tested whether inhibition of dilncRNA could affect this progression. We observed that 53BP1 foci progression was halted by transcription inhibition, with foci maturation arrested in the nucleation phase (when treatment started) and unable to enter the growth and coalescence phase (Fig. 7c and Movie 4), indicating that de novo transcription regulates 53BP1 foci physical properties throughout their temporal evolution. In addition, we tested the impact of antisense oligonucleotides (ASO) on formed 53BP1 foci. Both lipofection and microinjection of sequence-specific ASO against dilncRNA, but not control, in NIH2/4 cells, in which DSB can be induced at a known and traceable locus [5], caused 53BP1 focus disappearance (Fig. 7e, f and Movie 6). We next studied whether foci were disappearing as solid or liquid objects. By measuring the volume of the imaged 53BP1 foci and their average intensity, as a measure of their density, upon ASO treatments, we observed an average intensity dropping in a time scale 10 times faster than that associated with size reduction (Fig. 7e, f). This biophysical behaviour is typical of liquid/viscous objects and not of solid ones.

Overall, these results are consistent with 53BP1 foci being LLPS events dependent on dilncRNA throughout time.

RNA synthesis drives phase separation of 53BP1 at DSB *in vitro*

To further investigate the contribution of RNA to 53BP1 foci formation by LLPS, we exploited our previously-described *in vitro* system (Fig. 5a-d) with nuclear extracts from cells expressing 53BP1-GFP [42]. We noted that in those reactions containing H2AX and supplemented with the full set of rNTP, or cellular RNA, the solutions turned opaque (Fig. S5d). To test whether such increase in turbidity, often indicative of macromolecular phase transition, was due to droplets formation, we analysed the solutions by DIC and fluorescence microscopy. We observed that only the combination of H2AX-containing nucleosome arrays and rNTPs allowed the formation of 53BP1-GFP containing condensates (Fig. 8a).

Photobleaching of these condensates resulted in rapid and homogeneous liquid-like recovery (Fig. 8b) and addition of NH_4OAc disrupted them (Fig. 8a), supporting their nature as liquid compartments. Notably, while cellular RNA favoured droplet formation, such droplets were not 53BP1-GFP positive, demonstrating that cellular transcripts, not generated from H2AX-containing nucleosomes templates, did not make a significant contribution to the formation of 53BP1 condensates in this system (Fig. 8a). To further validate our *in vivo* observations on the role of PIC components and dilncRNAs, we tested the impact of transcriptional inhibitors or ASO against dilncRNA, or of antibodies against TBP and TFIIB. We observed that all these treatments prevented 53BP1-GFP droplets formation (Fig. 8c) and transcriptional inhibitors or ASO also disrupted them once already formed (Fig. 8d). We therefore demonstrated in a controlled *in vitro* system a role for PIC components and dilncRNA in promoting 53BP1 LLPS events.

Phase separation and de novo transcription impact on DSB repair

We previously reported that transcription inhibition or ASO against dilncRNA impair DSB repair[5]. To test the role of PIC components and LLPS events in DNA repair, we studied the impact of transcription inhibition by THZ1 and of phase separation disruption by ammonium acetate (NH_4OAc) [43] on DSB repair in irradiated HeLa cells by neutral comet assay; mirin, a MRN inhibitor[57] was used as a control. All these treatments resulted in increased comet tail moment, indicative of impaired DNA repair (Fig. 8e). In addition, we used EJ5-GFP U2OS cells[58] to monitor the effects of transcription or LLPS impairment on DNA repair through distal NHEJ, a pathway in which 53BP1 plays a key role[59]. By measuring the religation rates following the generation of two distant DSB [7] by genomic DNA qPCR, we observed a clear reduction of DNA repair efficacy in cells treated with the CDK7 inhibitor THZ1 or the LLPS inhibitor 1,6-hexanediol (Fig. 8f). DNA repair impairment was comparable to MRN inhibition by mirin, with the only difference that mirin was highly toxic in cut cells at day two.

Overall, these results show that PIC components and LLPS positively contribute to DSB repair.

Discussion

The DDR, including DNA damage signaling and repair, has been shown to be regulated by RNA in several independent reports [60] but the mechanisms of RNA synthesis, including the proteins involved, and whether unique to DSB or shared with other transcriptional apparatuses has remained unclear. Here we show that DSBs recruit the main subunits of PIC and Mediator complexes and elongation factor CDK9. Our results suggest a model whereby MRN recognizes DNA ends and recruits the PIC and Mediator complexes which, together with CDK9, promote POLR2A full activation. Inactivation of PIC components prevents RNAPII detection at DSB and transcription, impairing signalling and repair. Our results, supporting a linear cascade of events in which MRN recruits PIC that recruits RNAPII, may also be compatible with PIC and RNAPII mutually stabilizing each other at a DSB in an MRN-dependent manner. Either way, DSBs serve as sites of sequence-independent recruitment of transcriptional activity reminiscent of transcriptional promoters or enhancers.

Importantly, the function of PIC in DDR depends on its ability to fuel dilncRNA synthesis at DNA breaks, as best demonstrated in our *in vitro* system.

The notion that PIC components are recruited at DSB and are essential for full DDR activation by promoting RNA synthesis at DSB may have important consequences beyond mechanistic studies. CDK7 kinase inhibitors like THZ1 are presently considered cancer therapy candidates [39, 61, 62]: our results suggest that at least part of its effects on cancer cells, which tend to accumulate high levels of endogenous DNA damage [63], may be related to its impact on DDR.

How RNA transcribed from a damaged DNA template contributes to the secondary recruitment of DDR factors has been unclear since its discovery. Here we show that such RNA favors LLPS of the DDR foci component 53BP1. RNA has been shown to function as driving agent for protein condensation by promoting local concentration of RNA-interacting proteins [30] which can form liquid droplets through liquid-liquid demixing by phase separation. This event is likely to favour DNA damage signaling and repair events by controlling diffusion and concentration of DDR factors in proximity to DSBs. Notably, neither RNA nor γH2AX are sufficient to allow DDR foci formation alone: it is possible that γH2AX acts as a beacon recruiting DDR factors by protein-protein interactions [3] and RNA retains them at DSB through a web of multivalent low-specificity interactions, which may be additionally inducing structural changes favoring phase transition and condensates formation. A dynamic behavior for DDR foci was previously reported [42, 64, 65]. We now show that DDR foci exhibit liquid-like behaviors including nucleation, growth and coarsening equivalent to phase-separating fluids, behaving as viscous structures with spontaneous shape fluctuations set by an effective surface tension, they show rapid recovery from photobleaching, and are sensitive to agents that perturb liquid-like structures. By inhibiting transcription prior or during LLPS formation at DSB we concluded that RNA synthesis promotes faster molecular exchange and thus fluidity of 53BP1 compartments and controls their evolution in time. This result is consistent with reports on the emerging role of RNA in preventing increase in gelation of phase separated bodies [45, 46]. In particular, “maturation” or “hardening” is typical of IDR-based condensates that, initially fluid, may become more viscoelastic over time, eventually behaving as solids [24]. While our experiment with ASOs proved a crucial role for dilncRNA in promoting 53BP1 condensates formation and evolution, it is possible that they contribute in more than one way to LLPS at DSB. Indeed, DSB recruitment of RNF168 ubiquitin ligase is dependent on transcription [5] and ubiquitin has been shown to promote [66] and be promoted [67] by phase separation. In addition, the RNA binding protein FUS undergoes LLPS at DNA damage sites [31, 68], very early and transiently, and depending on poly(ADP-ribose) polymers [32], which, we note, are remarkably similar to RNA. PAR chains may transiently contribute to stabilize the transcription machinery at DSB, as suggested in other contexts [69].

Of note, LLPS may exert roles beyond foci formation and the reported ability of condensates to exert mechanical forces [70] together with our observed recruitment of MED1 at DSBs is intriguing and may suggests events akin to those reported at enhancers, also shown to engage LLPS [17, 20, 46], where distant genetic elements are brought in close proximity.

Europe PMC Funders Author Manuscripts

Supplementary Material

Refer to Web version on PubMed Central for supplementary material.

Acknowledgements

We thank N.G. Walter and S. Pitchiaya (Single Molecule Analysis Group and Center for RNA Biomedicine, Department of Chemistry, University of Michigan) for the generation of crucial preliminary data; all F.d'A.d.F group members for support and discussions; E. Soutoglou (Institut de Génétique et de Biologie Moléculaire et Cellulaire, Strasbourg and France), J. Lukas (Novo Nordisk Foundation Center for Protein Research, Copenhagen, Denmark.) for reagents; C. Zeirhut (Laboratory of Chromosome and Cell Biology, The Rockefeller University, New York) for reagents and discussions; F. Iannelli for bioinformatic analysis of repair products; S. Pasqualato of the Biochemistry and Structural Biology Unit at the European Institute of Oncology IRCCS, Milan, for the purifications of DNA fragments; F.P was supported by Marie Curie international mobility fellowship part of Structured International Post Doc Program (SIPOD); F.G. and R.C were supported by Regione Lombardia and CARIPLO foundation (Project-2016-0998); F.G. was supported by the Associazione Italiana per Ricerca sul Cancro, AIRC (MFAG 2018-22083); F.d'A.d.F. was supported by AIRC (application 12971 and 21091), Cariplo Foundation (grant 2014-0812), Fondazione Telethon (GGP17111), PRIN 2010-2011 and 2015, the Italian Ministry of Education Universities and Research EPIGEN Project, InterOmics Project and AMANDA project Accordo Quadro Regione Lombardia-CNR, a European Research Council advanced grant (322726), AriSLA (project `DDRNA and ALS') and AIRC Special Program 5 per mille metastases (Project-21091).

References

1. Jackson SP, Bartek J. The DNA-damage response in human biology and disease. Nature. 2009; 461:1071–1078. [PubMed: 19847258]
2. di Fagagna, FdA. Living on a break: cellular senescence as a DNA-damage response. Nature Reviews Cancer. 2008; 8:512. [PubMed: 18574463]
3. Ciccia A, Elledge SJ. The DNA damage response: making it safe to play with knives. Mol Cell. 2010; 40:179–204. [PubMed: 20965415]
4. Francia S, et al. Site-specific DICER and DROSHA RNA products control the DNA-damage response. Nature. 2012; 488:231–235. [PubMed: 22722852]
5. Michelini F, et al. Damage-induced lncRNAs control the DNA damage response through interaction with DDRNAs at individual double-strand breaks. Nat Cell Biol. 2017; 19:1400–1411. [PubMed: 29180822]
6. Francia S, Cabrini M, Matti V, Oldani A, d'Adda di Fagagna F. DICER, DROSHA and DNA damage response RNAs are necessary for the secondary recruitment of DNA damage response factors. J Cell Sci. 2016; 129:1468–1476. [PubMed: 26906421]
7. Gioia U, et al. Pharmacological boost of DNA damage response and repair by enhanced biogenesis of DNA damage response RNAs. Sci Rep. 2019; 9
8. D'Alessandro G, et al. BRCA2 controls DNA:RNA hybrid level at DSBs by mediating RNase H2 recruitment. Nat Commun. 2018; 9
9. Lu WT, et al. Drosha drives the formation of DNA:RNA hybrids around DNA break sites to facilitate DNA repair. Nat Commun. 2018; 9:532. [PubMed: 29416038]
10. Pryde F, et al. 53BP1 exchanges slowly at the sites of DNA damage and appears to require RNA for its association with chromatin. J Cell Sci. 2005; 118:2043–2055. [PubMed: 15840649]
11. Rossiello F, et al. DNA damage response inhibition at dysfunctional telomeres by modulation of telomeric DNA damage response RNAs. Nat Commun. 2017; 8
12. Haberle V, Stark A. Eukaryotic core promoters and the functional basis of transcription initiation. Nat Rev Mol Cell Biol. 2018; 19:621–637. [PubMed: 29946135]
13. Andersson R, Sandelin A, Danko CG. A unified architecture of transcriptional regulatory elements. Trends in Genetics. 2015; 31:426–433. [PubMed: 26073855]
14. Kornberg R. The molecular basis of eukaryotic transcription (Nobel Lecture). Angew Chem Int Ed Engl. 2007; 46:6956–6965. [PubMed: 17668892]
15. Vernimmen D, Bickmore WA. The Hierarchy of Transcriptional Activation: From Enhancer to Promoter. Trends Genet. 2015; 31:696–708. [PubMed: 26599498]

16. Lu H, et al. Phase-separation mechanism for C-terminal hyperphosphorylation of RNA polymerase II. Nature. 2018; 558:318–323. [PubMed: 29849146]
17. Sabari BR, et al. Coactivator condensation at super-enhancers links phase separation and gene control. Science. 2018
18. Cho WK, et al. Mediator and RNA polymerase II clusters associate in transcription-dependent condensates. Science. 2018
19. Boehning M, et al. RNA polymerase II clustering through carboxy-terminal domain phase separation. Nature Structural & Molecular Biology. 2018; 25:833–840.
20. Boija A, et al. Transcription Factors Activate Genes through the Phase-Separation Capacity of Their Activation Domains. Cell. 2018
21. Berry J, Weber SC, Vaidya N, Haataja M, Brangwynne CP. RNA transcription modulates phase transition-driven nuclear body assembly. Proc Natl Acad Sci U S A. 2015; 112:E5237–5245. [PubMed: 26351690]
22. Boeynaems S, et al. Protein Phase Separation: A New Phase in Cell Biology. Trends Cell Biol. 2018; 28:420–435. [PubMed: 29602697]
23. Shin Y, Brangwynne CP. Liquid phase condensation in cell physiology and disease. Science. 2017; 357
24. Banani SF, Lee HO, Hyman AA, Rosen MK. Biomolecular condensates: organizers of cellular biochemistry. Nat Rev Mol Cell Biol. 2017; 18:285–298. [PubMed: 28225081]
25. Hyman AA, Weber CA, Julicher F. Liquid-liquid phase separation in biology. Annu Rev Cell Dev Biol. 2014; 30:39–58. [PubMed: 25288112]
26. Kato M, et al. Cell-free formation of RNA granules: low complexity sequence domains form dynamic fibers within hydrogels. Cell. 2012; 149:753–767. [PubMed: 22579281]
27. Hnisz D, Shrinivas K, Young RA, Chakraborty AK, Sharp PA. A Phase Separation Model for Transcriptional Control. Cell. 2017; 169:13–23. [PubMed: 28340338]
28. Langdon EM, et al. mRNA structure determines specificity of a polyQ-driven phase separation. Science. 2018; 360:922–927. [PubMed: 29650703]
29. Li P, et al. Phase transitions in the assembly of multivalent signalling proteins. Nature. 2012; 483:336–340. [PubMed: 22398450]
30. Lin Y, Protter DS, Rosen MK, Parker R. Formation and Maturation of Phase-Separated Liquid Droplets by RNA-Binding Proteins. Mol Cell. 2015; 60:208–219. [PubMed: 26412307]
31. Patel A, et al. A Liquid-to-Solid Phase Transition of the ALS Protein FUS Accelerated by Disease Mutation. Cell. 2015; 162:1066–1077. [PubMed: 26317470]
32. Altmeyer M, et al. Liquid demixing of intrinsically disordered proteins is seeded by poly(ADP-ribose). Nature Communications. 2015; 6
33. Lee TI, Young RA. Transcription of eukaryotic protein-coding genes. Annu Rev Genet. 2000; 34:77–137. [PubMed: 11092823]
34. Rust MJ, Bates M, Zhuang X. Sub-diffraction-limit imaging by stochastic optical reconstruction microscopy (STORM). Nat Methods. 2006; 3:793–795. [PubMed: 16896339]
35. Sengupta P, et al. Probing protein heterogeneity in the plasma membrane using PALM and pair correlation analysis. Nat Methods. 2011; 8:969–975. [PubMed: 21926998]
36. Jao CY, Salic A. Exploring RNA transcription and turnover in vivo by using click chemistry. Proc Natl Acad Sci U S A. 2008; 105:15779–15784. [PubMed: 18840688]
37. Galbiati A, Beausejour C, d'Adda di Fagagna F. A novel single-cell method provides direct evidence of persistent DNA damage in senescent cells and aged mammalian tissues. Aging Cell. 2017; 16:422–427. [PubMed: 28124509]
38. Galbiati, A, d'Adda di Fagagna, F. DNA Damage In Situ Ligation Followed by Proximity Ligation Assay (DI-PLA)Cellular Senescence: Methods and Protocols. Demaria, M, editor. Springer New York; New York, NY: 2019. 11–20.
39. Wang Y, et al. CDK7-dependent transcriptional addiction in triple-negative breast cancer. Cell. 2015; 163:174–186. [PubMed: 26406377]

40. Lee KB, Wang D, Lippard SJ, Sharp PA. Transcription-coupled and DNA damage-dependent ubiquitination of RNA polymerase II in vitro. Proc Natl Acad Sci U S A. 2002; 99:4239–4244. [PubMed: 11904382]
41. Radebaugh CA, et al. TATA box-binding protein (TBP) is a constituent of the polymerase I-specific transcription initiation factor TIF-IB (SL1) bound to the rRNA promoter and shows differential sensitivity to TBP-directed reagents in polymerase I, II, and III transcription factors. Mol Cell Biol. 1994; 14:597–605. [PubMed: 8264628]
42. Bekker-Jensen S, Lukas C, Melander F, Bartek J, Lukas J. Dynamic assembly and sustained retention of 53BP1 at the sites of DNA damage are controlled by Mdc1/NFBD1. J Cell Biol. 2005; 170:201–211. [PubMed: 16009723]
43. Jain A, Vale RD. RNA phase transitions in repeat expansion disorders. Nature. 2017; 546:243–247. [PubMed: 28562589]
44. Liang L, Wang X, Xing D, Chen T, Chen WR. Noninvasive determination of cell nucleoplasmic viscosity by fluorescence correlation spectroscopy. J Biomed Opt. 2009; 14
45. Elbaum-Garfinkle S, et al. The disordered P granule protein LAF-1 drives phase separation into droplets with tunable viscosity and dynamics. Proc Natl Acad Sci U S A. 2015; 112:7189–7194. [PubMed: 26015579]
46. Nair SJ, et al. Phase separation of ligand-activated enhancers licenses cooperative chromosomal enhancer assembly. Nat Struct Mol Biol. 2019; 26:193–203. [PubMed: 30833784]
47. Kroschwald S, Maharana S, Simon A. Hexanediol: a chemical probe to investigate the material properties of membrane-less compartments. Matters. 2017; 3
48. Strom AR, et al. Phase separation drives heterochromatin domain formation. Nature. 2017; 547:241–245. [PubMed: 28636597]
49. Onuki, A. Phase transition dynamics. Cambridge University Press; 2002.
50. Voorhees PW. Ostwald ripening of two-phase mixtures. Annual Review of Materials Science. 1992; 22:197–215.
51. Zwicker D, Decker M, Jaensch S, Hyman AA, Julicher F. Centrosomes are autocatalytic droplets of pericentriolar material organized by centrioles. Proc Natl Acad Sci U S A. 2014; 111:E2636–2645. [PubMed: 24979791]
52. Berry J, Brangwynne CP, Haataja M. Physical principles of intracellular organization via active and passive phase transitions. Rep Prog Phys. 2018; 81
53. Caragine CM, Haley SC, Zidovska A. Surface Fluctuations and Coalescence of Nucleolar Droplets in the Human Cell Nucleus. Phys Rev Lett. 2018; 121
54. Jeng U-S, Esibov L, Crow L, Steyerl A. Viscosity effect on capillary waves at liquid interfaces. Journal of Physics: Condensed Matter. 1998; 10:4955.
55. Gang H, Krall AH, Weitz DA. Shape fluctuations of interacting fluid droplets. Phys Rev Lett. 1994; 73:3435–3438. [PubMed: 10057380]
56. Brangwynne CP, et al. Germline P granules are liquid droplets that localize by controlled dissolution/condensation. Science. 2009; 324:1729–1732. [PubMed: 19460965]
57. Dupre A, et al. A forward chemical genetic screen reveals an inhibitor of the Mre11-Rad50-Nbs1 complex. Nat Chem Biol. 2008; 4:119–125. [PubMed: 18176557]
58. Gunn A, Stark JM. I-SceI-based assays to examine distinct repair outcomes of mammalian chromosomal double strand breaks. Methods Mol Biol. 2012; 920:379–391. [PubMed: 22941618]
59. Difilippantonio S, et al. 53BP1 facilitates long-range DNA end-joining during V(D)J recombination. Nature. 2008; 456:529–533. [PubMed: 18931658]
60. Michelini F, et al. From “Cellular” RNA to “Smart” RNA: Multiple Roles of RNA in Genome Stability and Beyond. Chem Rev. 2018; 118:4365–4403. [PubMed: 29600857]
61. Chipumuro E, et al. CDK7 inhibition suppresses super-enhancer-linked oncogenic transcription in MYCN-driven cancer. Cell. 2014; 159:1126–1139. [PubMed: 25416950]
62. Christensen CL, et al. Targeting transcriptional addictions in small cell lung cancer with a covalent CDK7 inhibitor. Cancer Cell. 2014; 26:909–922. [PubMed: 25490451]
63. Di Micco R, et al. Oncogene-induced senescence is a DNA damage response triggered by DNA hyper-replication. Nature. 2006; 444:638. [PubMed: 17136094]

64. Dimitrova N, Chen Y-CM, Spector DL, de Lange T. 53BP1 promotes non-homologous end joining of telomeres by increasing chromatin mobility. Nature. 2008; 456:524. [PubMed: 18931659]
65. Aymard F, et al. Genome-wide mapping of long-range contacts unveils clustering of DNA double-strand breaks at damaged active genes. Nat Struct Mol Biol. 2017; 24:353–361. [PubMed: 28263325]
66. Sun D, Wu R, Zheng J, Li P, Yu L. Polyubiquitin chain-induced p62 phase separation drives autophagic cargo segregation. Cell Res. 2018; 28:405–415. [PubMed: 29507397]
67. Bouchard JJ, et al. Cancer Mutations of the Tumor Suppressor SPOP Disrupt the Formation of Active, Phase-Separated Compartments. Mol Cell. 2018; 72:19–36 e18. [PubMed: 30244836]
68. Rulten SL, et al. PARP-1 dependent recruitment of the amyotrophic lateral sclerosis-associated protein FUS/TLS to sites of oxidative DNA damage. Nucleic Acids Res. 2014; 42:307–314. [PubMed: 24049082]
69. Krishnakumar R, Kraus WL. PARP-1 regulates chromatin structure and transcription through a KDM5B-dependent pathway. Mol Cell. 2010; 39:736–749. [PubMed: 20832725]
70. Shin Y, et al. Liquid Nuclear Condensates Mechanically Sense and Restructure the Genome. Cell. 2019; 176:1518. [PubMed: 30849377]

Europe PMC Funders Author Manuscripts

Europe PMC Funders Author Manuscripts

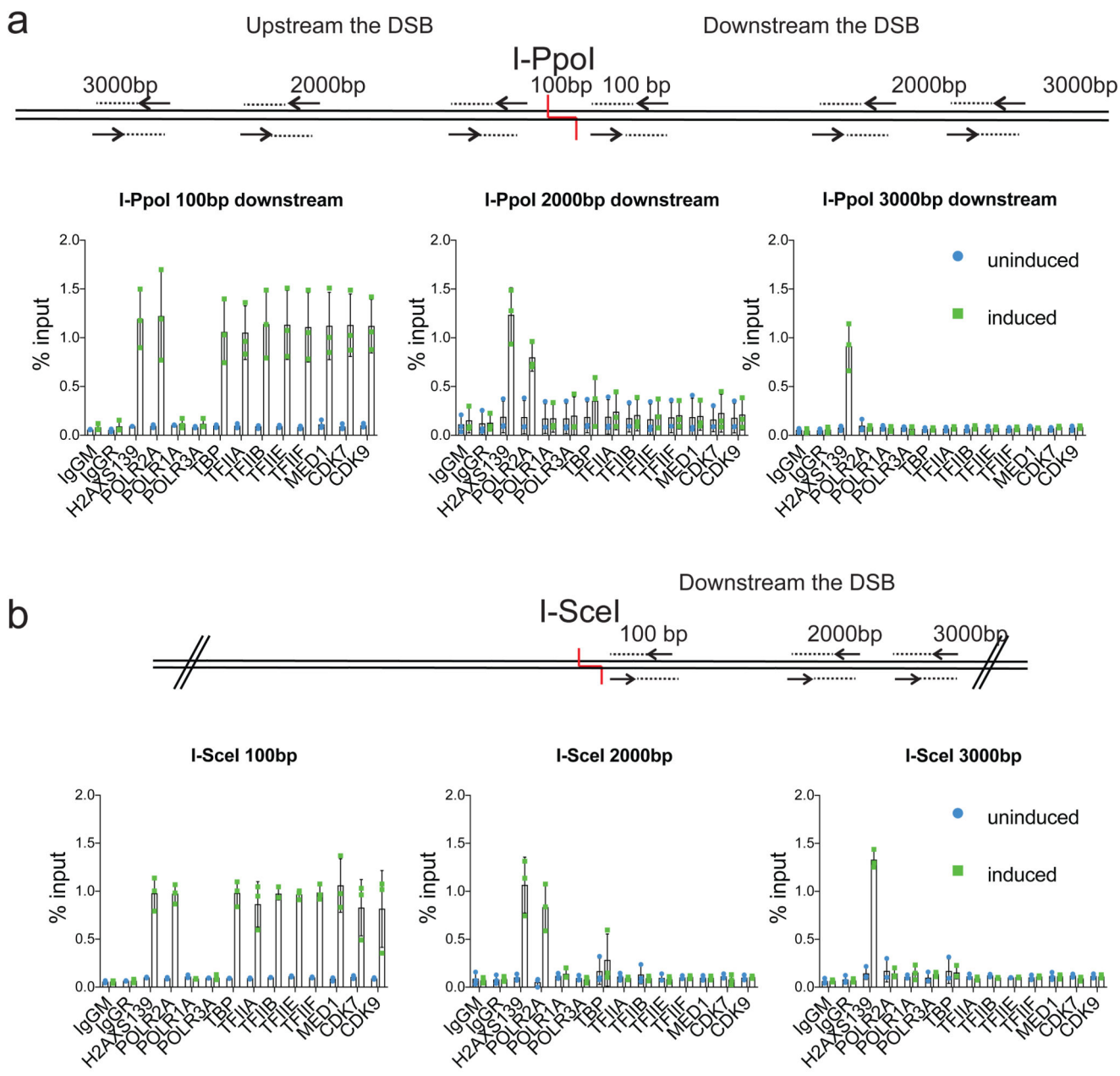

Figure 1. RNAPII and PIC are recruited to DSBs as detected by ChIP *in vivo*.

(a) Schematic representation of the endogenous genomic locus studied. Annealing positions of primer pairs used for ChIP-qPCR with distances relative to the cut site are shown. Bar plots show percentage of enrichment relative to the input of γH2AX, POLR2A, POLR1A, POLR3A, PIC components, MED1 and CDK9 as detected by ChIP at 100bp, 2000bp and 3000bp downstream the DSB induced by I-PpoI at DAB1 locus. N=3 independent experiments. (b) Schematic representation of the engineered locus studied. Annealing positions of primer pairs used for ChIP-qPCR with distances relative to the cut site are shown. Bar plots show percentage of enrichment relative to the input of γH2AX, POLR2A, POLR1A, POLR3A, PIC components, MED1 and CDK9 as detected by ChIP at 100bp,

2000bp and 3000bp distances from the DSB induced by I-SceI at an engineered locus in HeLa ptight cell line. N=3 independent experiments. Statistics source data are provided in Supplementary Table 2.

Europe PMC Funders Author Manuscripts

Europe PMC Funders Author Manuscripts

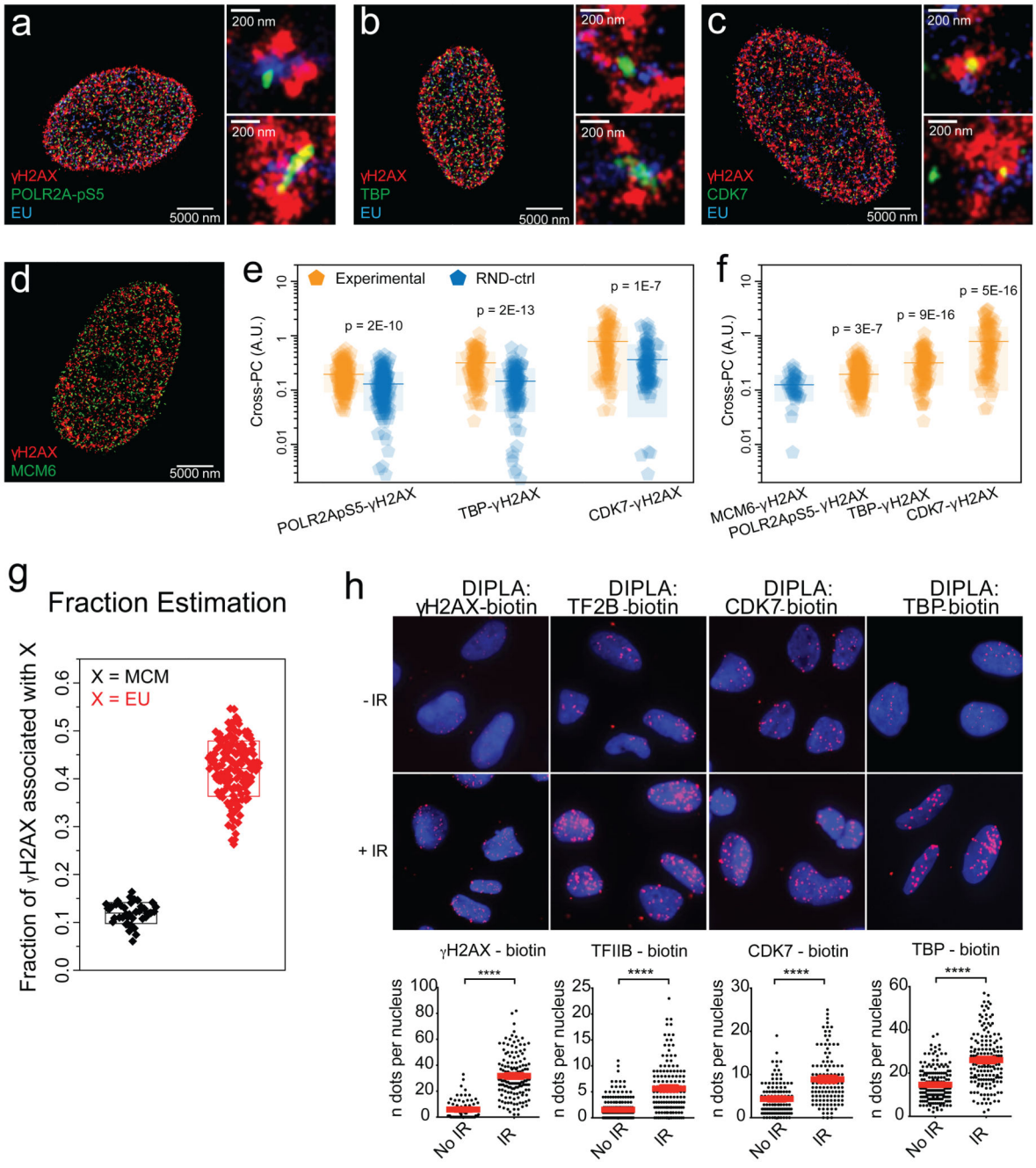

Figure 2. RNAP II and PIC components localize to DSB as detected by super-resolution imaging and DI-PLA.

(a-c) U2OS cells treated with NCS for 30 minutes and labelled with EU (15 minutes pulse) were analysed by super-resolution imaging. Representative images of γH2AX and EU stainings with: POLR2A-pS5 (a) and PIC components TBP (b) and CDK7 (c). Experiments were repeated independently 4, 3 and 3 times respectively. (d) Representative image of γH2AX and MCM6 in U2OS nucleus treated with NCS for 30 minutes. Experiment was repeated independently 2 times (e-f) Statistical analysis of the Cross-PC between POLR2A-pS5/TBP/CDK7 and γH2AX as compared to their self-randomized correlation signal (RND-

ctrl, e), or to the correlation between MCM6 and γH2AX (f). The box indicates mean +/- SD. n=184, 109, 102, and 40 nuclei were collected from 4, 3, 3, and 2 biologically independent experiments for cross-PC analyses between POLR2A-pS5/TBP/CDK7/MCM and γH2AX, respectively. P-values of the two-sample unpaired t-test were shown in the figure accordingly. (g) Fraction of γH2AX colocalizing either with MCM (black, negative control) or EU (red). Box denotes mean +/- SD (n=40 and 162 nuclei collected from 2 and 4 biologically independent experiments for MCM and EU, respectively). The p-value of the two-sample unpaired t-test is $2E\text{-}10^{6}$. (h) DI-PLA between biotin and TFIIB, CDK7, TBP or γH2AX in U2OS cells irradiated (2Gy) and analyzed 30 minutes later or untreated (- IR). Each plot represents at least 80 nuclei analyzed and error bars show the SEM of N=3 biologically independent experiments. P values were calculated by unpaired t-test and significance are represented as * P<0.05, ** P<0.01, *** P<0.001, **** P<0.0001. Representative images are shown in the upper panels. Statistics source data are provided in Supplementary Table 2.

Europe PMC Funders Author Manuscripts

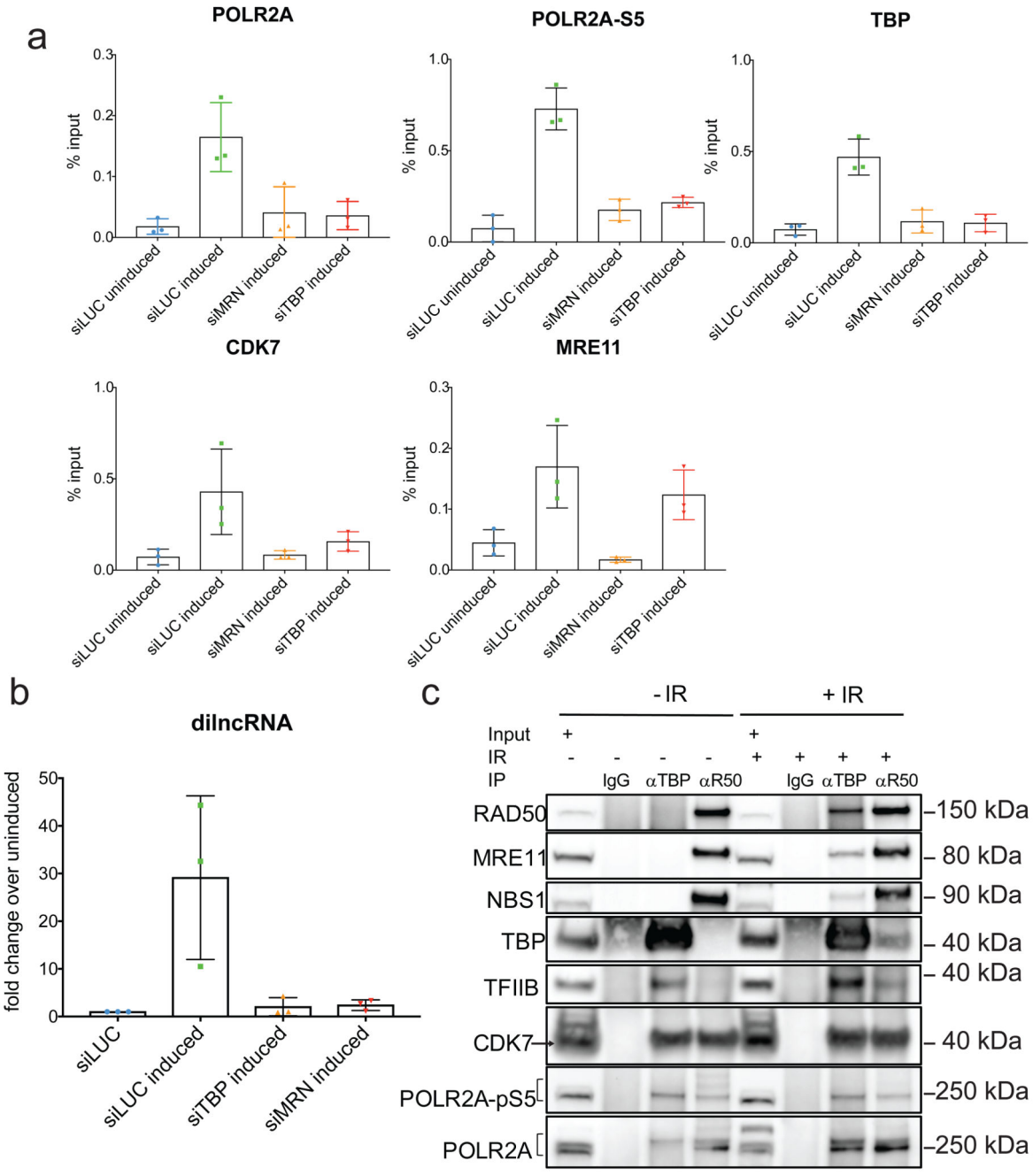

Figure 3. MRN complex controls PIC recruitment at endogenous DSB.

(a) Bar plot shows percentage of enrichment relative to input of POLR2A, POLR2ApS5, TBP, CDK7, MRE11 as detected at the DAB1 locus by ChIP at 100bp from the DSB induced by I-PpoI in HeLa cells knocked down for MRN (siMRN), TBP (siTBP) or Luciferase (siLuc) as negative control. N=3 independent experiments. (b) Induction of dilncRNAs by I-PpoI cut measured by strand-specific RT-qPCR in HeLa cells knocked down for MRN (siMRN), TBP (siTBP) or Luciferase (siLuc) as negative control. Bar plots show mean of enrichment of the indicated RNA sets upon DSB, relative to uncut. N=3

independent experiments. (c) Co-immunoprecipitation of TBP and RAD50 following IR exposure. HEK293T cells were irradiated (+ IR) or not (- IR) and samples were collected 10 min post IR, followed by immunoprecipitation of individual component of the MRN complex (RAD50) and PIC (TBP). Whole-cell extract (Input) and immunoprecipitated samples were analysed by immunoblotting. Mouse immunoglobulins (IgG) were used as control. This experiment was repeated twice with similar results. Statistics source data are provided in Supplementary Table 2.

Europe PMC Funders Author Manuscripts

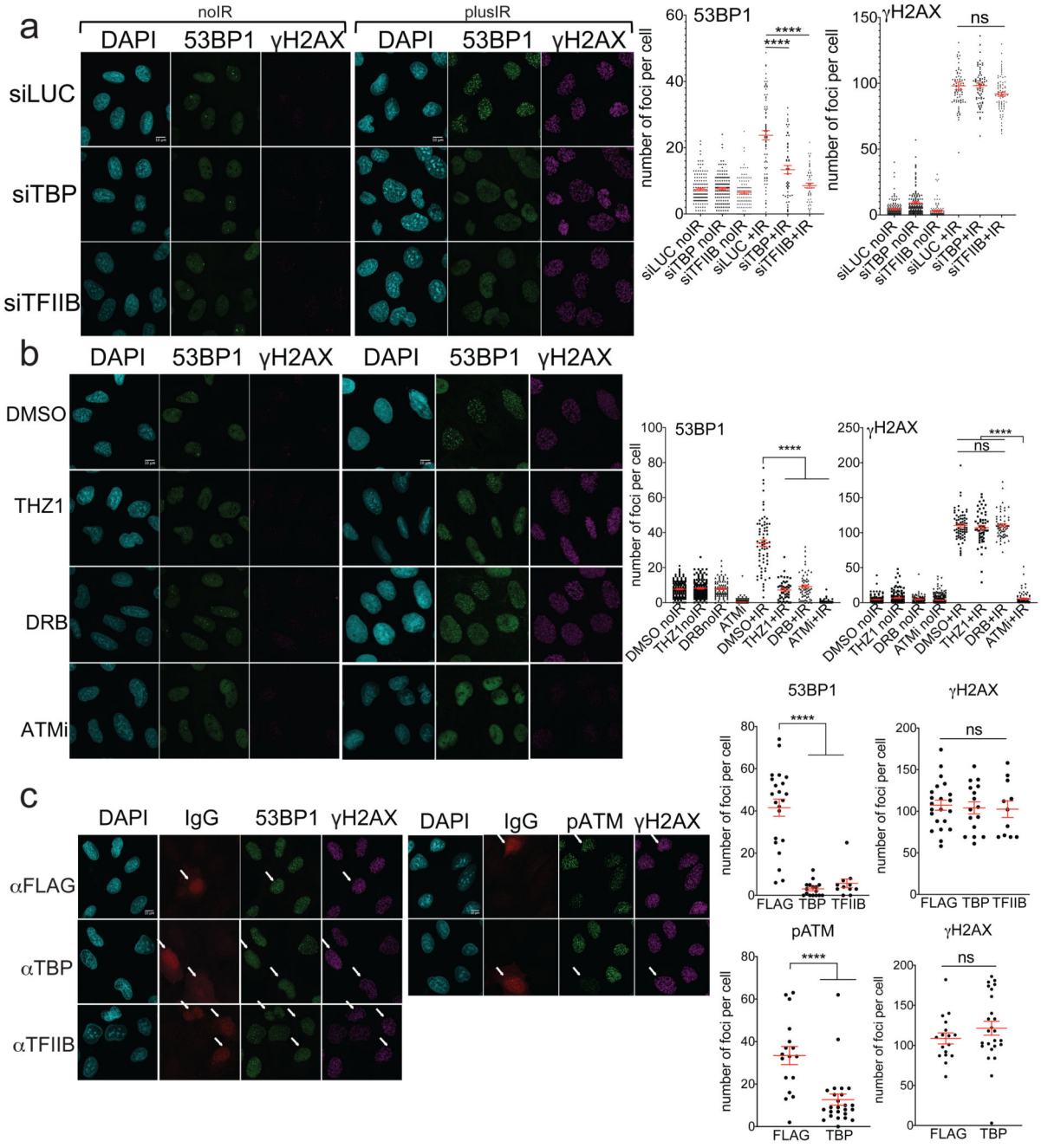

Figure 4. PIC inactivation by RNA interference, small molecules or inhibitory antibodies reduces DDR signaling in cultured cells.

(a) Knock down by siRNAs of indicated proteins in U2OS cells which were exposed to IR (1 Gy, plusIR) or not (noIR), fixed 15 minutes afterwards and immunostained. Foci formation of indicated DDR factors were visualized and quantified. In each plot error bars show the SEM of n=131 siLUCnoIR, n=131 siTBPnoIR, n=108 siTFIIBnoIR, n=190 siLUC+IR, n=151 siTBP+IR, n=153 siTFIIB+IR nuclei analyzed from 1 (noIR) or 3 (plusIR) biologically independent experiments. γH2AXplusIR quantifications are the pool of dataset from Figure 4a, S4a-b. P values were calculated by one-way ANOVA test and significance

Europe PMC Funders Author Manuscripts

are represented as * P<0.05, ** P<0.01, *** P<0.001, **** P<0.0001. (b) U2OS cells treated with DMSO, THZ1, DRB or ATMi for 30 min were exposed to IR (1 Gy, plusIR) or not (noIR). 15 minutes after irradiation cells were fixed and immunostained. Foci formation of indicated DDR factors was visualized and quantified. Each plot show error bars and the SEM of n=139 DMSOnoIR, n=129 THZ1noIR, n=84 DRBnoIR, n=270 ATMinoIR, n=104 DMSO+IR, n=90 THZ1+IR, n=117 DRB+IR, n=133 ATMi+IR nuclei analyzed from 1 (noIR) or 2 (plusIR) biologically independent experiments. γH2AX plus IR quantifications are the pool of dataset from Figure 4b, S4f. P values were calculated by one-way ANOVA test and significance are represented as * P<0.05, ** P<0.01, *** P<0.001, **** P<0.0001. (c) Antibodies against regulatory domains of TBP or TFIIB proteins were microinjected into U2OS cells nuclei (indicated by white arrows), 20 minutes later cells were irradiated (1 Gy) and after 15 additional minutes fixed and immunostained. Foci formation of the indicated DDR factors was visualized and quantified in injected cells identified by staining against microinjected antibodies. Quantifications represent the SEM of number of foci per IgG-positive nucleus detected and analized. P values were calculated by unpaired t-test and significance are represented as **** P<0.0001. *(left)* 53BP1 experiment: FLAG 22 nuclei, TBP 17 nuclei, TFIIB 11 nuclei. *(right)* pATM experiment: FLAG 17 nuclei, TBP 25 nuclei. Statistics source data are provided in Supplementary Table 2.

Europe PMC Funders Author Manuscripts

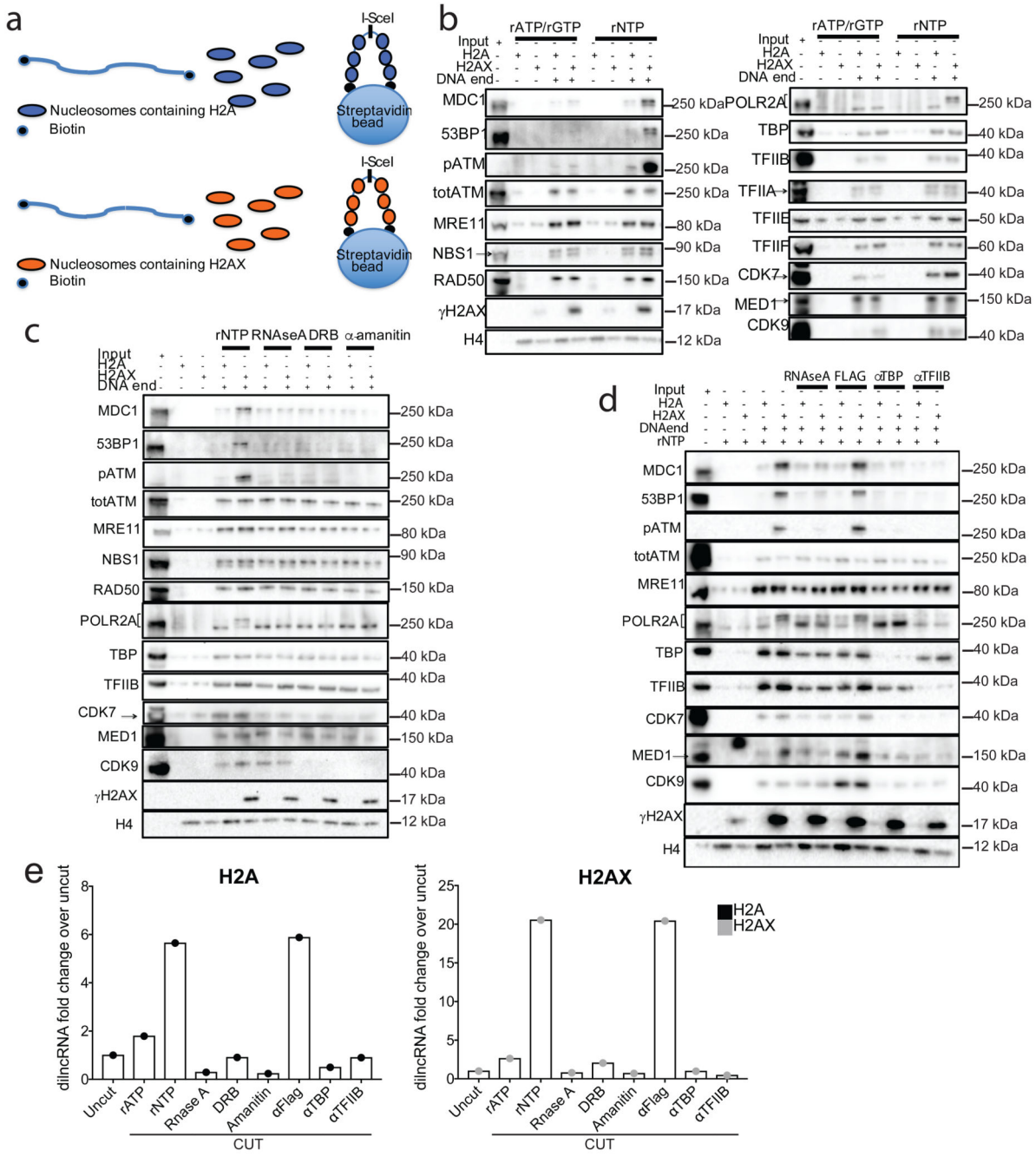

Figure 5. An *in vitro* assay demonstrates a role of PIC and of RNA synthesis in DDR factors recruitment at DSB.

(a) Recombinant nucleosomes containing either H2A or H2AX were immobilized on streptavidin beads, either mock treated or cut with I-SceI endonuclease and then incubated with HeLa nuclear extract. (b-d) Immunoblottings of the indicated proteins associated with nucleosomes in different conditions are shown: (b) Recruitment of DDR factors at chromatinized DSBs assayed in the presence of rATP/rGTP only (no transcription) or in the presence of the full set of rNTPs (transcription allowed); (c) Recruitment of DDR factors at chromatinized DSBs assayed upon: RNA degradation by RNAseA, transcription inhibition

by DRB and α-amanitin; (d) Recruitment of DDR factors at chromatinized DSBs assayed in presence of antibodies against the regulatory domains of TBP and TFIIB proteins, or FLAG as negative control. Experiments were repeated twice with similar results. (e) A tenth of the *in vitro* reactions from panels a-c was used to measure dilncRNA synthesis by strand-specific RT-qPCR. N=1 per experiment. Statistics source data are provided in Supplementary Table 2.

Europe PMC Funders Author Manuscripts

Europe PMC Funders Author Manuscripts

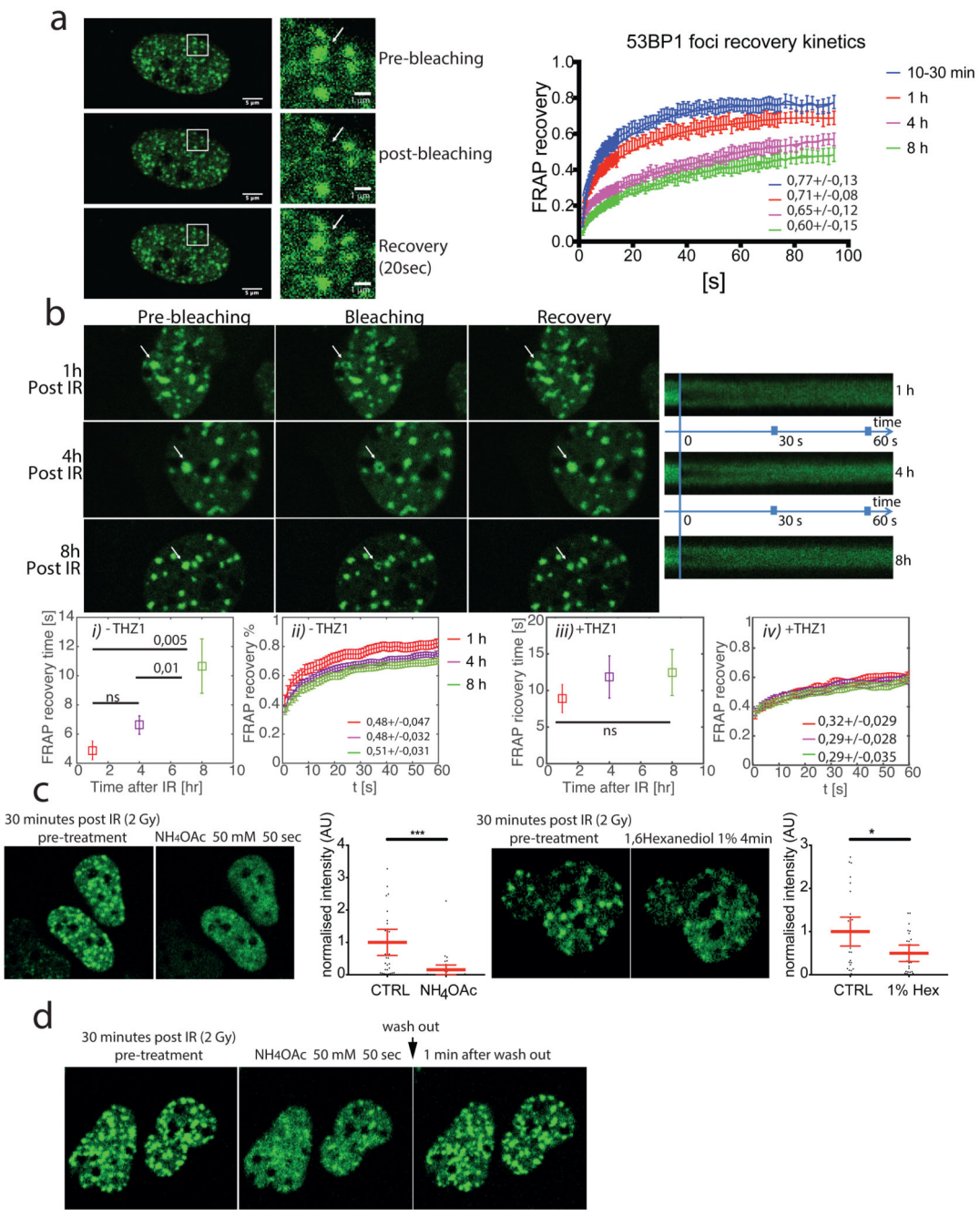

Figure 6. 53BP1 DDR foci are RNA-dependent liquid-liquid demixed condensates.

(a) *Left:* Representative images of FRAP of a 53BP1-GFP focus after 30 minutes from irradiation (2 Gy) *Right:* FRAP analysis of 53BP1-GFP foci in U2OS cells at different time points after IR (2 Gy). Error bars represent the SD on N=18 (10min), 10 (1h), 8 (h), 5 (8h) nuclei from 2 biologically independent experiments. One-way ANOVA test scored a significance P-value <0.0001. In the graph the mean of mobile fractions and the SD are shown for each sample. (b) Representative images of partial FRAP within 53BP1-GFP foci in time. Kymograph on the right shows internal bleaching and homogeneous internal

recovery of a representative bleached focus. Time of recovery and SD of internally bleached foci after 1 hour (10 foci), 4 hours (17 foci) and 8 hours (11 foci) from irradiation (2Gy) is shown in lower graph *(i).* Recovery kinetic of the same foci is shown *(ii).,* Data are from 2 biologically independent experiments. P-values of unpaired t-test are also shown. In the graph the mean of mobile fractions and the SD are shown for each sample. *(iii, iv)* 53BP1-GFP foci were analyzed in the same conditions as *(i)* and *(ii)* but THZ1 100nM was added 30 minutes before each timepoint. In the graph the mean of mobile fractions and the SD are shown for each sample. (c) U2OS cells expressing 53BP1-GFP were irradiated (2 Gy), 30 minutes after IR were treated with 50mM NH_4OAc or 1% 1,6-hexanediol (Hex) and observed by timelapse live microscopy. Representative screenshots and quantification of 53BP1-GFP foci intensity are shown. Error bars represent the means ± 95% CI of from at least 3 independent experiments, at least 25 nuclei were scored per condition. P values are expressed as * $P<0.05$, *** $P<0.001$. (d) U2OS cells expressing 53BP1 GFP were irradiated and 30 minutes after IR (2Gy) cells were treated with 50mM NH_4OAc. After 1 minute fresh medium was added and NH_4OAc diluted to 10mM. Representative snapshots are shown. Experiment was repeated at least 3 times with similar results. Statistics source data are provided in Supplementary Table 2.

Europe PMC Funders Author Manuscripts

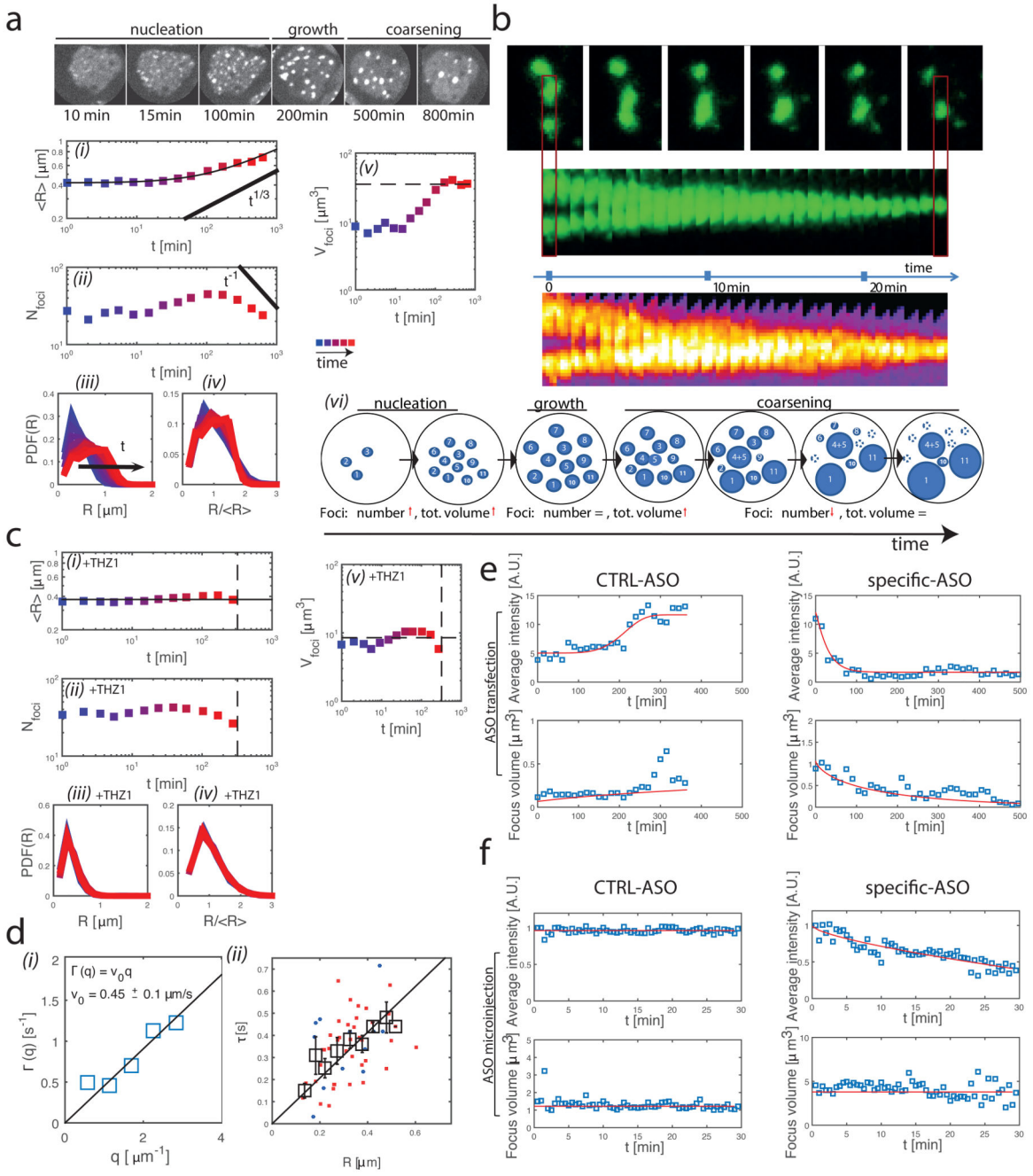

Figure 7. Biophysical properties of 53BP1 condensates.

(a, b) U2OS cells expressing 53BP1-GFP were irradiated (2 Gy) and analysed (>20 nuclei from 2 independent experiments) by timelapse live microscopy for 12 hours starting 10 minutes post IR. (a) *Above:* Representative snapshots from Movie 2 illustrating the kinetic of 53BP1-GFP foci formation. *Below: (i)* Symbols: temporal evolution of the average radius of the foci. Continuous thin line: best fit to the data with the function $[K(t + t_0)]^n$, the best fitting exponent being: $n = 0.29 \pm 0.05$, compatible with the value 1/3 expected in both DLC and BMC scenarios. *(ii)* Symbols: temporal evolution of the average number of foci per

nucleus. *(iii)* Frequency distributions of foci radius measured at different time points (logarithmically spaced between 1 and 700 min). *(iv)* Same as in *(iii)*, with both axes rescaled with the average radius. A nice collapse of all curves onto an invariant distribution is observed for t >100min. *(v)* Symbols: temporal evolution of the total volume of foci per nucleus (estimated as $\frac{4}{3}\pi N_{foci}\langle R\rangle^3$). *(vi)* Pictorial representation of the proposed model of 53BP1 foci kinetic through LLPS. (b) Example of coalescence of 53BP1 foci (above) and associated kymograph (below). (c) 53BP1-GFP U2OS cells were treated and analyzed as in (a) but 30 minutes after IR THZ1 100nM was added. (d) *(i)* Decorrelation rate Γ(q) obtained from Fourier analysis of droplet shape fluctuations as a function of the wave-vector q (see also Fig S6c). Γ(q) follows the dispersion relation expected for overdamped capillary waves and provides an estimate of the propagation speed v_0=0.45±0.1 μm/s. *(ii)* Characteristic lifetime τ of shape fluctuations as a function of the foci size as obtained from intensity correlation analysis. Each red (blue) circle corresponds to one focus measured 4 hours (8 hours) after irradiation (n=51 foci). Black boxes: average τ calculated by binning the data over intervals of width 0.05 μm, bars: associated standard error. (e-f) Average intensity and volume of 53BP1-GFP single foci upon treatment with sequence-specific ASO and control ASO (CTRL). (e) Transfection experiment was repeated twice with similar results. (f) Microinjection experiment was repeated 4 times with similar results. Statistics source data are provided in Supplementary Table 2.

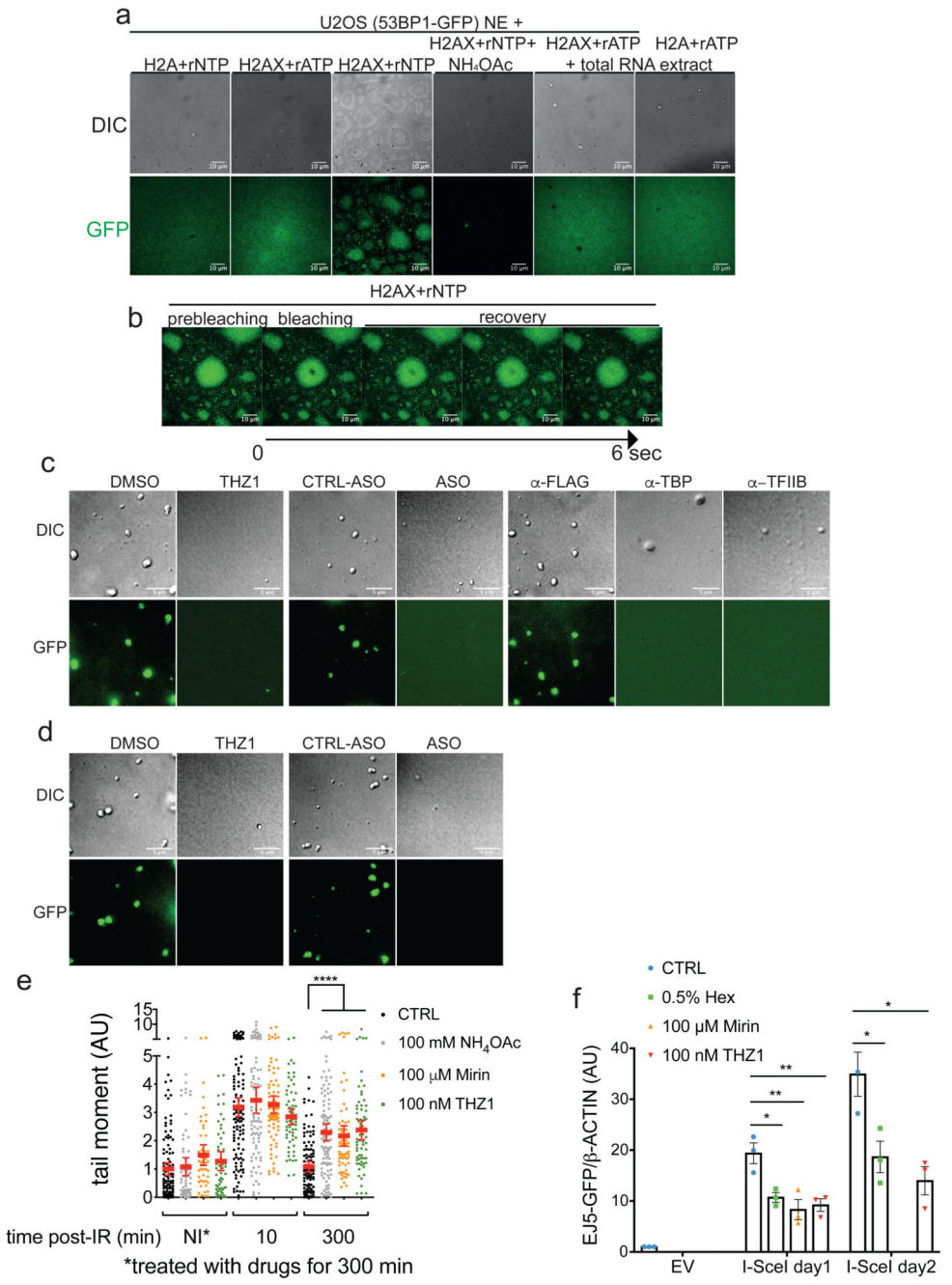

Figure 8. 53BP1 forms droplets *in vitro* in a transcription-dependent manner and 53BP1 LLPS is important for DSB repair in cells.

(a) Representative images of droplet formation in U2OS 53BP1-GFP nuclear extract. Both DIC and GFP (FITC) channels are shown. Experiment was repeated twice with similar results. (b) FRAP of internal fraction of a 53BP1-GFP condensate and snapshots of recovery are shown. Experiment was repeated twice with similar results. (c) Representative images of droplet formation in U2OS 53BP1-GFP nuclear extract. H2AX-containing nucleosomes and rNTPs were added to trigger the reaction and immediately treated as indicated. Both DIC and GFP (FITC) channels are shown. N=1. (d) Representative images of droplet formation

in U2OS 53BP1-GFP nuclear extract treated as indicated. H2AX-containing nucleosomes and rNTPs were added to trigger the reaction and, after droplets formation, treated as indicated. Both DIC and GFP (FITC) channels are shown. N=1. (e) DNA repair kinetics were monitored by neutral comet-assay at different time-points post-IR (5Gy) in HeLa cells. Not irradiated (NI) cells treated with the drugs for 5 h (300 min) and untreated control cells (CTRL) are also shown. The dot plot shows quantification of IR-induced DSBs by tail moment analysis. Red bars indicate average values ± 95% CI of CTRL NI n=116, 10min n=113, 300min n=114, NH_4OAc NI n=69, 10min n=88, 300min n=108, Mirin NI n=50, 10min n=89, 300min n=71, THZ1 NI n=54, 10min n=61, 300min n=70 cells per sample from three independent experiments. (f) EJ5-GFP U2OS cells were transfected with an I-SceI-expressing plasmid or with an empty vector (EV) and concomitantly treated with the indicated drugs. Untreated cells (CTRL) were used as control. DSB re-joining events were evaluated by qPCR (EJ5-GFP) on genomic DNA collected at 24 or 48 h after plasmid transfection; *β-ACTIN* gene was used as reference. Repair efficiency is shown relative to untreated cells transfected with the EV and represented as the means ± s.e.m. of n=3 independent experiments. (e-f) P values were calculated by one-way ANOVA and significance are represented as * P<0.05, ** P<0.01, **** P<0.0001. Statistics source data are provided in Supplementary Table 2.

Europe PMC Funders Author Manuscripts